J Intell Robot Syst (2012) 66:303–319
DOI 10.1007/s10846-011-9595-z

New Potential Functions with Random Force Algorithms Using Potential Field Method

Jinseok Lee · Yunyoung Nam · Sangjin Hong · Weduke Cho

Received: 31 October 2010 / Accepted: 26 April 2011 / Published online: 12 July 2011

Abstract Autonomous mobile robot path planning is a common topic for robotics and computational geometry. Many important results have been found, but a lot of issues are still veiled. This paper first describes new problem of symmetrically aligned robot-obstacle-goal (SAROG) when using potential field methods for mobile robot path planning. In addition, we consider constant robot speed for practical use. The SAROG and the constant speed involve two potential risks: robot-obstacle collision and local minima trap. For dealing with the two potential risks, we analyze the conditions of the collision and the local minima trap, and propose new potential functions and random force based algorithms. For the algorithm verification, we use WiRobot X80 with three ultrasonic range sensor modules.

Keywords Potential function · Navigation · SAROG · Obstacle avoidance

J. Lee
Department of Biomedical Engineering,
Worcester Polytechnic Institute,
Worcester, MA 01609, USA
e-mail: jinseok@wpi.edu

Y. Nam · S. Hong (✉)
Department of Electrical and Computer Engineering,
Stony Brook University, Stony Brook,
NY 11794-2350, USA
e-mail: snjhong@ece.sunysb.edu

Y. Nam
e-mail: yynam@ece.sunysb.edu

W. Cho
Department of Electrical and Computer Engineering,
Ajou University, Suwon, 443-749, Korea
e-mail: chowd@ajou.ac.kr

1 Introduction

Autonomous navigation of a robot relies on the ability of the robot to achieve its goal with obstacle avoidance. In some cases, a robot has a complete knowledge of its environment, and plans its movement based on it. However, in general, the robot only has an idea about the goal, and should reach it using its sensors to gather information about the environment. Hierarchical systems decompose the control process by functions, and low-level processes provide simple functions that are grouped together by higher-level processes in order to provide overall vehicle control [1]. Thus, high level processing is a planning level, and low level processing is a reactive control. This is called local path planning. The local path planning should be performed with the local information only near a robot in real time, and it takes priority over the high level plans. Therefore, it is sometimes called real time obstacle avoidance. One of the local path planning methods is the potential field method.

The potential field method has been widely studied for autonomous mobile robot path planning, whose purpose is that a robot reaches a goal with obstacle avoidance by potential levels [2, 3]. The principle of the potential field method is that an obstacle exerts a repulsive force onto a robot while a goal applies an attractive force to a robot [4]. One of the reasons for the popularity of the method is its simplicity and mathematical elegance. In addition, the method is applicable when a robot does not have a-priori model of an obstacle. However, the method has some inherent limitations such as local minima trap. The trap situations occur when a robot runs into a dead end, and a robot never reaches a goal [5]. Many attempts for the local minima escape or avoidance have been made in a variety of ways [6–9].

In the previous studies, [10] used harmonic functions with Laplace's equation for eliminating the local minima. The method effectively obviates the local minima problem, but the solution for the Laplace equation should be provided. Rimon and Koditscheck [11] eliminated the local minima by filling up the entire local minima region. However, the method should search the local minima and update the new potential field in real time. Hence, it is not appropriate for real time motion planning. Such new potential functions have been actively proposed [3, 5, 12, 13]. Together with the new potential functions, multi-potential functions were also considered [14]. In the method, when a local minima is found in one potential field, another potential map with different resolution ignores the local minima. However, the method has limitation which a robot may move back to a previously visited region with local minima.

Together with the new potential functions, random path planner approaches have been proposed [15, 16]. In the approaches, potential field methods drive the search for a path in configuration space with the help of a suitable heuristic function; they combine gradient-based and goal-oriented motions with random movements to escape local minima. However, the approach was reported that a robot may move back to previously explored region [17]. In addition, the approach is affected by attraction force; and thus, the number of steps required to escape from a local minima is unknown.

In this paper, we restrict two conditions. One condition is that a robot has a constant speed and determines its direction every sampling time. As a robot moves with constant speed with every sampling time, the computational complexity is reduced. In addition, it is more practical to adopt a constant speed with sampling time. The other condition is that a robot, an obstacle and a goal are symmetrically aligned. Such order placement is one of the most challenging issues of local minima trap. Recently, the method using virtual obstacle [6, 18, 19] has been widely used for local minima escape. However, in the method, the positions and shapes of a robot and an obstacle are non-aligned and/or asymmetric. For instance, [6] presented the

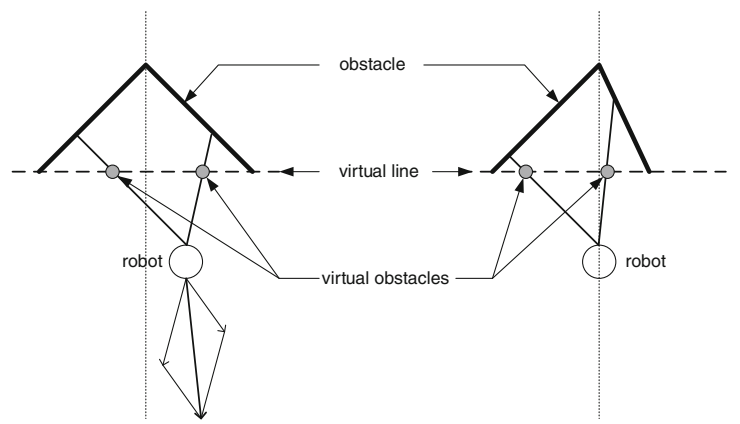

Fig. 1 The virtual obstacle concept for the minimal local trap escape

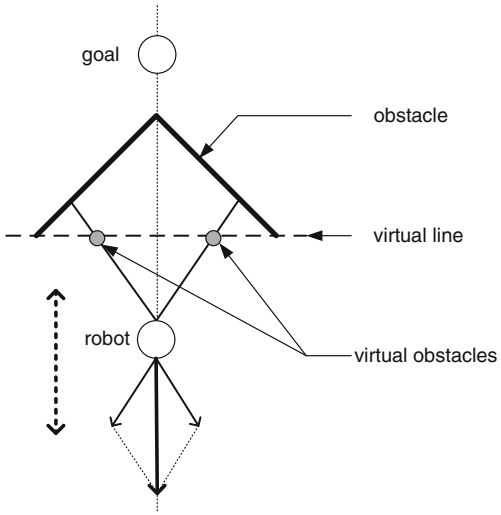

Fig. 2 Illustration of symmetrically aligned robot-obstacle-goal (SAROG): the virtual obstacles symmetrically exert the repulsive forces on a robot

virtual obstacle concept for the minimal local trap escape as illustrated in Fig. 1. The escape from the minimal local trap is valid when the virtual obstacles are asymmetrically formed with respect to a robot. On the other hand, when the virtual obstacles symmetrically exert the repulsive forces on a robot, and a goal is positioned aligned with the obstacle and the robot as illustrated in Fig. 2, the robot moves back and forth only by endlessly falling into the local minima trap. We refer to the problem of symmetrically aligned robot-obstacle-goal as SAROG. In a previous study, the symmetrically aligned robot-obstacle-goal (SAROG) was addressed and solved by implementing ER1 robot [20]. However, it has an assumption that the robot has limited possible moving direction with the predefined grids. Since the robot moves to only one of eight neighbor positions, the method does not fully take an advantage of potential field.

Throughout this paper, we address problems and solutions on the restricted two conditions of SAROG and robot constant speed. Figure 3 illustrates two problems based on SAROG and constant speed: local minima trap and robot-obstacle collision. For simplicity, the problems are depicted by representing a robot, an obstacle and a goal with a point mass in two-dimension coordinates. In case of the local minima trap, a robot moves back and forth between the two positions A and B. In the position A, the attractive force is stronger than the repulsive force. On the other hand, in the position B, the repulsive force is stronger than the attractive force. In case of the robot-obstacle collision, the attractive and repulsive force inequality of A' and B' is same as that of A and B, but the distance between A' and the obstacle is shorter than the robot movement.

For dealing with the problems of local minima trap and the robot-obstacle collision on the conditions of SAROG and robot constant speed, we propose new potential functions and random force based algorithms. The new potential functions aim at avoiding the robot-obstacle collision. The random force based algorithm aims at escaping the local minima trap.

The remainder of this paper has five sections. Section 2 briefly explains the potential field method and describes problems corresponding to SAROG and constant speed. In Section 3, we propose new potential functions and random force algorithms for collision avoidance and local minim

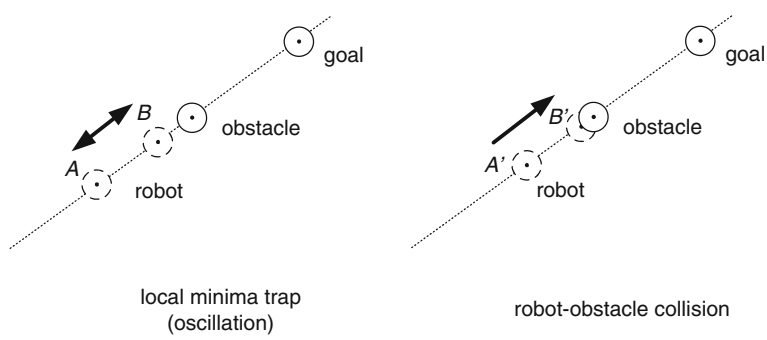

Fig. 3 Illustration of the two problems based on SAROG and constant speed: local minima trap and robot-obstacle collision

trap escape. Section 4 verifies the proposed algorithm using WiRobot X80. Finally, our contribution is summarized in Section 5.

2 Potential Field Method and SAROG Problem

2.1 Potential Field Methods

A robot, an obstacle and a goal are represented by a point mass in two-dimension coordinates. Given a space with size $X_s \times Y_s$, each position is denoted by

$$\mathbf{p} = [x \;\; y]^T, \tag{1}$$

where $0 \le x \le X_s$ and $0 \le y \le Y_s$. Each position of a robot, an obstacle and a goal are denoted by

$$\mathbf{p}_r = [x_r \;\; y_r]^T, \;\; \mathbf{p}_o = [x_o \;\; y_o]^T \text{ and } \mathbf{p}_g = [x_g \;\; y_g]^T. \tag{2}$$

In the potential field method, an attractive potential is defined as a function of the relative distance between a robot and a goal while a repulsive potential is defined as a function of the relative distance between a robot and an obstacle. The two potential functions are commonly expressed as [4, 7, 21, 22]

$$U_{\text{att}}(\mathbf{p}) = c_{\text{att}} \cdot \big(\rho(\mathbf{p}, \mathbf{p}_g)\big)^m, \tag{3}$$

and

$$U_{\text{rep}}(\mathbf{p}) = \begin{cases} c_{\text{rep}} \cdot \left(\dfrac{1}{\rho(\mathbf{p}, \mathbf{p}_o)} - \frac{1}{\rho_0}\right)^n, & \text{if } 0 < \rho(\mathbf{p}, \mathbf{p}_o) \le \rho_0 \\ 0, & \text{if } \rho(\mathbf{p}, \mathbf{p}_o) > \rho_0 \\ H, & \text{if } \rho(\mathbf{p}, \mathbf{p}_o) = 0 \end{cases}, \tag{4}$$

where c_{att} and c_{rep} are constant values for an attractive potential and a repulsive potential, H denotes the highest value that microprocessor possesses. $\rho(\mathbf{p}, \mathbf{p}_g) = ||\mathbf{p}, \mathbf{p}_g||$ is the shortest distance between two positions, $\mathbf{p}$ and $\mathbf{p}_g$. Similarly, $\rho(\mathbf{p}, \mathbf{p}_o) = ||\mathbf{p}, \mathbf{p}_o||$ is the shortest distance between two positions, $\mathbf{p}$ and $\mathbf{p}_o$. ρ_0 is a positive constant denoting the distance influence of an obstacle. m and n are positive integer constants. For $m = n = 1$, each potential is conic in shape, and for $m = n = 2$, each potential is parabolic in shape.

The corresponding attractive force and repulsive force are then given by the negative gradient of each attractive potential and repulsive potential as

$$\begin{aligned} \mathbf{F}_{\text{att}}(\mathbf{p}) &= -\nabla U_{\text{att}}(\mathbf{p}) \\ &= -m \cdot c_{\text{att}} \cdot \Big(\rho(\mathbf{p}, \mathbf{p}_g)\Big)^{m-1} \cdot \nabla\rho\big(\mathbf{p}, \mathbf{p}_g\big), \end{aligned} \tag{5}$$

and

$$\begin{aligned} &\mathbf{F}_{\text{rep}}(\mathbf{p}) \\ &= -\nabla U_{\text{rep}}(\mathbf{p}) \\ &= \begin{cases} n \cdot c_{\text{rep}} \cdot \left(\dfrac{1}{\rho(\mathbf{p}, \mathbf{p}_o)} - \dfrac{1}{\rho_0}\right)^{n-1} \\ \quad \cdot \left(\dfrac{1}{\rho(\mathbf{p}, \mathbf{p}_o)}\right)^2 \\ \quad \cdot \nabla\rho(\mathbf{p}, \mathbf{p}_o), & \text{if } 0 < \rho(\mathbf{p}, \mathbf{p}_o) \le \rho_0 \\ \mathbf{0}, & \text{if } \rho(\mathbf{p}, \mathbf{p}_o) > \rho_0 \\ & \quad \text{or } \rho(\mathbf{p}, \mathbf{p}_o) = 0 \end{cases}, \end{aligned} \tag{6}$$

where $\mathbf{0}$ denotes two dimensional zero vector, $\nabla\rho(\mathbf{p}, \mathbf{p}_o)$ and $\nabla\rho(\mathbf{p}, \mathbf{p}_g)$ are two unit vectors pointing from $\mathbf{p}_o$ to $\mathbf{p}$ and from $\mathbf{p}_g$ to $\mathbf{p}$, respectively. That is, the two unit vectors are expressed as

$$\nabla\rho(\mathbf{p}, \mathbf{p}_o) = \begin{cases} \mathbf{0}, & \text{if } x = x_o \text{ and } y = y_o \\ \dfrac{(x - x_o)\mathbf{u}_x + (y - y_o)\mathbf{u}_y}{\sqrt{(x - x_o)^2 + (y - y_o)^2}}, & \text{otherwise} \end{cases}, \tag{7}$$

$$\nabla\rho(\mathbf{p}, \mathbf{p}_g) = \begin{cases} \mathbf{0}, & \text{if } x = x_g \text{ and } y = y_g \\ \dfrac{(x - x_g)\mathbf{u}_x + (y - y_g)\mathbf{u}_y}{\sqrt{(x - x_g)^2 + (y - y_g)^2}}, & \text{otherwise} \end{cases}, \tag{8}$$

where $\mathbf{u}_x$ and $\mathbf{u}_y$ are unit vectors in x and y direction, respectively.

The total force applied to each position $\mathbf{p}$ is the sum of the attractive force and the repulsive force as

$$\mathbf{F}_{\text{tot}}(\mathbf{p}) = \mathbf{F}_{\text{att}}(\mathbf{p}) + \mathbf{F}_{\text{rep}}(\mathbf{p}), \tag{9}$$

which determines the robot direction and speed for reaching a goal with obstacle avoidance. The robot direction is the summed vector of $\nabla\rho(\mathbf{p}, \mathbf{p}_g)$ and $\nabla\rho(\mathbf{p}, \mathbf{p}_o)$. As mentioned in the previous section, we consider that a robot moves with constant speed. Thus, the total force $\mathbf{F}_{\text{tot}}(\mathbf{p})$ can be reformulated as

$$\begin{aligned}&\mathbf{F}^c_{\text{tot}}(\mathbf{p})\\ &= \frac{\mathbf{F}_{\text{tot}}(\mathbf{p})}{|\mathbf{F}_{\text{tot}}(\mathbf{p})|}\\ &= \begin{cases}\mathbf{0}, & \text{if } \mathbf{F}_{\text{att}}(\mathbf{p}) = \mathbf{F}_{\text{rep}}(\mathbf{p}) = 0\\ \dfrac{\mathbf{F}_{\text{att}}(\mathbf{p}) + \mathbf{F}_{\text{rep}}(\mathbf{p})}{|\mathbf{F}_{\text{att}}(\mathbf{p}) + \mathbf{F}_{\text{rep}}(\mathbf{p})|}, & \text{otherwise}\end{cases},\end{aligned} \tag{10}$$

where $\mathbf{F}^c_{\text{tot}}$ is the total force in the condition of constant robot speed. Then, given the speed s_r (m/s) and sampling time T_s (s), a robot moves $s_r \cdot T_s$ with the direction of $\mathbf{F}^c_{\text{tot}}(\mathbf{p})$ or $(\mathbf{F}_{\text{att}}(\mathbf{p}) + \mathbf{F}_{\text{rep}}(\mathbf{p}))/(|\mathbf{F}_{\text{att}}(\mathbf{p}) + \mathbf{F}_{\text{rep}}(\mathbf{p})|)$ every T_s. Figure 4 illustrates the forces $\mathbf{F}_{\text{tot}}(\mathbf{p}_r)$ and $\mathbf{F}^c_{\text{tot}}(\mathbf{p}_r)$ onto a robot by addition of the attractive force $\mathbf{F}_{\text{att}}(\mathbf{p}_r)$ and the repulsive force $\mathbf{F}_{\text{rep}}(\mathbf{p}_r)$. Throughout this paper, we call $\mathbf{F}^c_{\text{tot}}$ a unit total force. Similarly, we call $\mathbf{F}^c_{\text{att}}$ and $\mathbf{F}^c_{\text{rep}}$ a unit attractive force and a unit repulsive force.

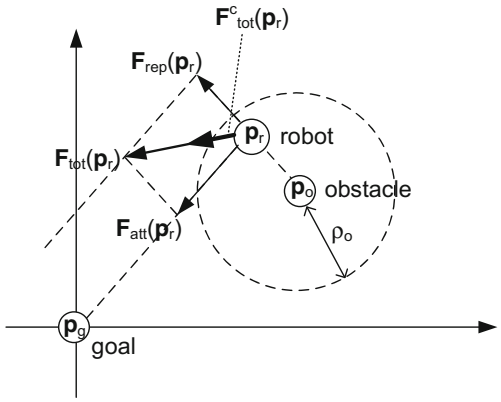

Fig. 4 Illustration of the forces $\mathbf{F}_{\text{tot}}(\mathbf{p}_r)$ and $\mathbf{F}^c_{\text{tot}}(\mathbf{p}_r)$ onto a robot by addition of the attractive force $\mathbf{F}_{\text{att}}(\mathbf{p}_r)$ and the repulsive force $\mathbf{F}_{\text{rep}}(\mathbf{p}_r)$ using the potential field method. On the condition of constant speed, we use unit forces of $\mathbf{F}^c_{\text{tot}}$, $\mathbf{F}^c_{\text{att}}$ and $\mathbf{F}^c_{\text{rep}}$

2.2 Problem Description

On the two conditions of constant robot speed and SAROG, the potential field method causes two problems: collision and local minima trap.

As illustrated in Fig. 5, if $|\mathbf{F}_{\text{att}}(\mathbf{p}_r)| > |\mathbf{F}_{\text{rep}}(\mathbf{p}_r)|$ and $\rho(\mathbf{p}_r, \mathbf{p}_o) \le s_r \cdot T_s$, the robot collides with an obstacle at the next sampling time. Then the collision problem condition is summarized as

$$|\mathbf{F}_{\text{att}}(\mathbf{p}_r)| > |\mathbf{F}_{\text{rep}}(\mathbf{p}_r)|, \tag{11}$$

$$\rho(\mathbf{p}_r, \mathbf{p}_o) \le s_r \cdot T_s, \tag{12}$$

$$\nabla\rho(\mathbf{p}_r, \mathbf{p}_o) = \nabla\rho(\mathbf{p}_r, \mathbf{p}_g). \tag{13}$$

On the other hand, if $|\mathbf{F}_{\text{att}}(\mathbf{p}_r)| < |\mathbf{F}_{\text{rep}}(\mathbf{p}_r)|$, a robot moves away from a goal and an obstacle until $|\mathbf{F}_{\text{att}}(\mathbf{p}_r)| > |\mathbf{F}_{\text{rep}}(\mathbf{p}_r)|$. Then the robot moves back toward an obstacle and a goal, and finally oscillates between two positions. The local minima problem condition is summarized as

$$|\mathbf{F}_{\text{att}}(\mathbf{p}_r)| > |\mathbf{F}_{\text{rep}}(\mathbf{p}_r)|, \tag{14}$$

$$\rho(\mathbf{p}_r, \mathbf{p}_o) > s_r \cdot T_s, \tag{15}$$

$$\nabla\rho(\mathbf{p}_r, \mathbf{p}_o) = \nabla\rho(\mathbf{p}_r, \mathbf{p}_g). \tag{16}$$

To illustrate the local minima problem, a simple simulation example is provided. Consider a robot moves with $s_r = \sqrt{2}$ and $T_s = 1$; a robot moves $\sqrt{2}$ every sampling time in the condition of $\mathbf{p}_o = [8\ \ 8]^T$ and $\mathbf{p}_g = [6\ \ 6]^T$. Both a robot and a goal

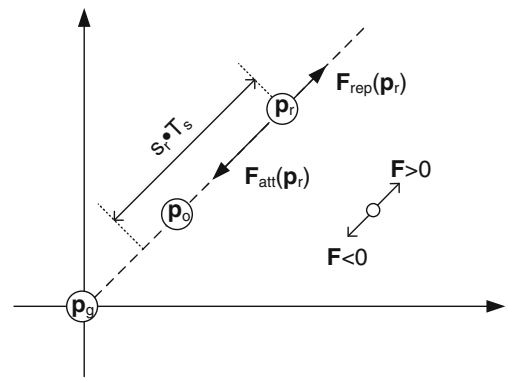

Fig. 5 The distance between a robot and an obstacle is less than $s_r T_s$

are within the distance of influence of an obstacle with ρ_o=10. The attractive potential and repulsive potential are specifically given by [8]

$$U_{\text{att}}(\mathbf{p}) = \frac{1}{2}\left(\rho(\mathbf{p}, \mathbf{p}_g)\right)^2, \tag{17}$$

$$U_{\text{rep}}(\mathbf{p}) = 5\left(\frac{1}{\rho(\mathbf{p}, \mathbf{p}_o)} - \frac{1}{10}\right)^2. \tag{18}$$

Note that $m = 2, n = 2, c_{\text{att}} = 0.5$ and $c_{\text{rep}} = 5$ are used in a general form of Eqs. 3 and 4. Their corresponding attractive force and repulsive force are obtained as

$$\mathbf{F}_{\text{att}}(\mathbf{p}) = -\rho(\mathbf{p}, \mathbf{p}_g) \cdot \nabla\rho(\mathbf{p}, \mathbf{p}_g), \tag{19}$$

$$\mathbf{F}_{\text{rep}}(\mathbf{p}) = 10\left(\frac{1}{\rho(\mathbf{p}, \mathbf{p}_o)} - \frac{1}{10}\right) \cdot \left(\frac{1}{\rho(\mathbf{p}, \mathbf{p}_o)}\right)^2 \cdot \nabla\rho(\mathbf{p}, \mathbf{p}_o). \tag{20}$$

Figure 6 shows the attractive force, the repulsive force and the total force in a diagonal line from (2, 2) to (14, 14). In this example, for better understanding, each force direction away from an origin is denoted as positive, and each force direction toward an origin is denoted as negative. From the goal position (6, 6), the attractive force is symmetrically exerted as shown in Fig. 6a. From the obstacle position (8, 8), the repulsive force is symmetrically exerted as shown in Fig. 6b. Note that the attractive force is a function of a goal position and a robot position while the repulsive force is a function of an obstacle position and a robot position. By addition of the attractive and repulsive forces, the total force is shown in Fig. 6c, where the total forces from (14, 14) to (8.9, 8.9) are negative, which causes a robot to move toward an obstacle. Suppose that a robot is initially positioned as $\mathbf{p}_r = [12 \quad 12]^T$, where the attractive and repulsive forces are −8.485 and +0.024, respectively. Then, the robot moves toward an origin (toward to the goal and the obstacle), and arrives at (11, 11). Again, at the position (11, 11), the attractive and repulsive forces are −7.071 and +0.075, respectively, and the robot moves toward an origin (toward to the goal and the obstacle). In this way, the robot keeps moving to (8, 8), which means the robot collides with the obstacle positioned at (8, 8). For another case, suppose that a robot is initially positioned as $\mathbf{p}_r = [11.5 \quad 11.5]^T$. At the position (11.5, 11.5), the attractive and repulsive forces are −7.778 and +0.042, respectively. Then, the robot moves toward an origin (toward to the goal and

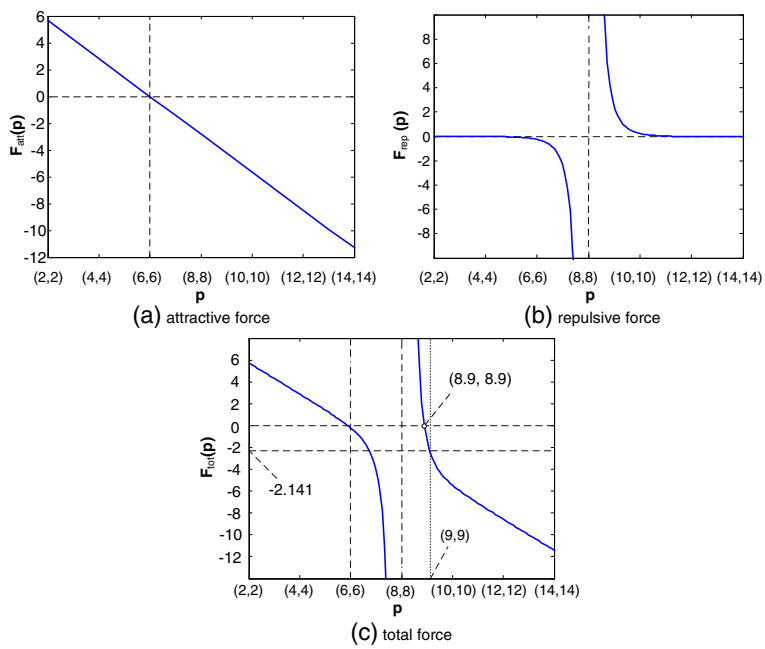

Fig. 6 The attractive force, the repulsive force and the total force in a diagonal line from (2, 2) to (14, 14)

the obstacle) and arrives at (10.5, 10.5). In this way, the robot keeps moving to (8.5, 8.5). At the position (8.5, 8.5), the attractive and repulsive forces are −3.536 and +26.284, respectively, and the robot moves away from an origin (away from the goal and the obstacle). Once the robot arrives at (9.5, 9.5), the robot is exerted by negative force (toward to the goal and the obstacle), and moves to (8.5, 8.5). Again, the robot is exerted by positive force (away from the goal and the obstacle) at (8.5, 8.5), and moves back to (9.5, 9.5). Finally, the robot oscillates the two positions between (9.5, 9.5) and (8.5, 8.5), which means the robot is trapped in local minima.

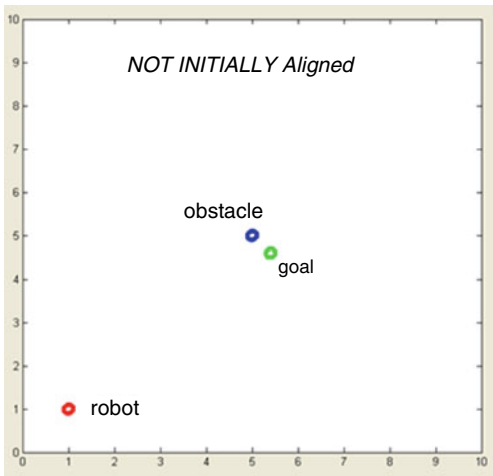

(a) Time-instant 0: arobotis positioned at (1.0,1.0), an obstacle is positioned at (5.0,5.0) and a goal is positioned at (5.4,4.6).

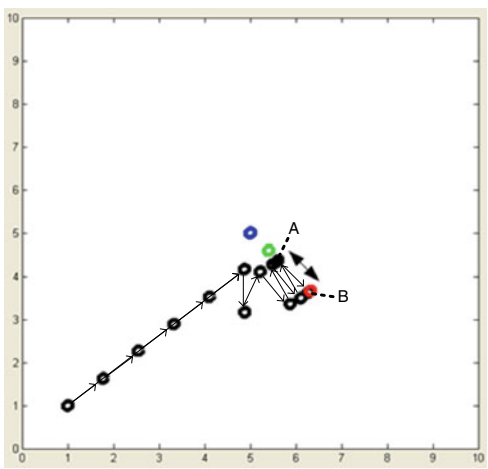

(b) From time-instant 13, a robot is oscillating between the points A and B (local minima trap).

Fig. 7 The SAROG based local minima occurs even when a robot, an obstacle and a goal are not initially aligned

The collision and local minima problems on the condition of constant robot speed and SAROG have not been addressed yet, and it should be taken into account to prevent a robot from damage by collision and the local minima trap (oscillation).

A question arises that the condition of SAROG can be negligible if a robot is not initially aligned with an obstacle and a goal. However, the SAROG occurs even when a robot, an obstacle and a goal are not initially aligned. As illustrated in Fig. 7, consider that a robot is initially positioned at (1.0 m, 1.0 m), an obstacle is positioned at (5.0 m, 5.0 m), and a goal is positioned at (5.4 m, 4.6 m). A robot speed s_r is $\sqrt{2}$ m/s, and sampling time T_s is 1 s. In addition, we set up $m = 2$, $n = 2$, $\rho = 1$, $c_{\text{att}} = 0.5$ and $c_{\text{rep}} = 5$. Throughout this paper, unless otherwise noted, the parameters s_r, T_s, m, n, ρ, c_{att} and c_{rep} are fixed as above.

As shown in Fig. 7a, at the sampling time 0, a robot, an obstacle and a goal are not initially aligned. However, when a robot moves closer to a goal, a robot finally oscillates between two points A and B by not reaching a goal as illustrated in Fig. 7b. That is, a robot, an obstacle and a goal become symmetrically aligned. Thus, the SAROG may occur when an obstacle and a goal closely positioned even though the initial positions of a robot, an obstacle and a goal are not aligned.

3 Collision Avoidance and Local Minim Escape on SAROG and Constant Speed

3.1 New Potential Functions For Collision Avoidance

For the robot collision avoidance, new potential functions should be considered. It should be derived to reflect the fact the collision arises based on the conditions of Eqs. 11–13. Then, the collision is avoided by imposing a unit force with an

opposite direction onto a robot when the collision conditions are satisfied. It motivates us to consider a new total force as

$$\mathbf{F}_{\text{tot}}(\mathbf{p}) = \begin{cases} \nabla\rho(\mathbf{p}_r, \mathbf{p}_o), & \text{if } |\mathbf{F}_{\text{att}}(\mathbf{p}_r)| > |\mathbf{F}_{\text{rep}}(\mathbf{p}_r)|, \\ & \quad \& \ \rho(\mathbf{p}_r, \mathbf{p}_o) \le s_r \cdot T_s \\ & \quad \& \ \nabla\rho(\mathbf{p}_r, \mathbf{p}_o) = \nabla\rho(\mathbf{p}_r, \mathbf{p}_g) \\ \mathbf{F}_{\text{att}}(\mathbf{p}) + \mathbf{F}_{\text{rep}}(\mathbf{p}), & \text{elsewhere}, \end{cases} \tag{21}$$

and the corresponding unit total force is expressed as

$$\mathbf{F}^c_{\text{tot}}(\mathbf{p}) = \begin{cases} \nabla\rho(\mathbf{p}_r, \mathbf{p}_o), & \text{if } |\mathbf{F}_{\text{att}}(\mathbf{p}_r)| > |\mathbf{F}_{\text{rep}}(\mathbf{p}_r)|, \\ & \quad \& \ \rho(\mathbf{p}_r, \mathbf{p}_o) \le s_r \cdot T_s \\ & \quad \& \ \nabla\rho(\mathbf{p}_r, \mathbf{p}_o) \\ & \quad\quad = \nabla\rho(\mathbf{p}_r, \mathbf{p}_g) \\ \mathbf{0}, & \text{if } \mathbf{F}_{\text{att}}(\mathbf{p}_r) = \mathbf{F}_{\text{att}}(\mathbf{p}_r) = \mathbf{0} \\ \dfrac{\mathbf{F}_{\text{att}}(\mathbf{p}) + \mathbf{F}_{\text{rep}}(\mathbf{p})}{|\mathbf{F}_{\text{att}}(\mathbf{p}) + \mathbf{F}_{\text{rep}}(\mathbf{p})|}, & \text{elsewhere}. \end{cases} \tag{22}$$

In comparison with Eq. 9, the new total force and the corresponding new unit total force ensure that a robot moves away from an obstacle before it is collided with an obstacle. In the previously shown example, the new total force replaces an original one by a unit vector pointing away from an obstacle as shown in Fig. 8. By using Eq. 22, when a robot moves from the position (10, 10) to the position (9, 9), it moves back to the position (10, 10), and the collision is avoided.

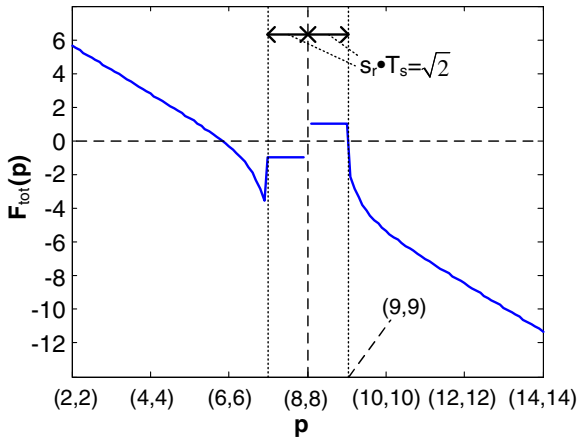

Fig. 8 The new total force based on Eq. 21 imposes a unit force with an opposite direction onto a robot in order that a robot moves away from an obstacle before it is collided with an obstacle

As the new total force in Eq. 21 is considered, each size of robot and an obstacle becomes an important parameter. We assume that a robot and an obstacle are circles in shape with radius r_r and r_o, respectively. Then, the distance $s_r \cdot T_s$ for obstacle avoidance is extended to $s_r \cdot T_s + r_r + r_o$. Then, the new total force and unit total force are revised as

$$\mathbf{F}_{\text{tot}}(\mathbf{p}) = \begin{cases} \nabla\rho(\mathbf{p}_r, \mathbf{p}_o), & \text{if } |\mathbf{F}_{\text{att}}(\mathbf{p}_r)| > |\mathbf{F}_{\text{rep}}(\mathbf{p}_r)|, \\ & \quad \& \ |\mathbf{p}_r - \mathbf{p}_0| \le s_r \cdot T_s + r_r + r_o \\ & \quad \& \ \nabla\rho(\mathbf{p}_r, \mathbf{p}_o) = \nabla\rho(\mathbf{p}_r, \mathbf{p}_g) \\ \mathbf{F}_{\text{att}}(\mathbf{p}) + \mathbf{F}_{\text{rep}}(\mathbf{p}), & \text{elsewhere}, \end{cases} \tag{23}$$

and

$$\mathbf{F}^c_{\text{tot}}(\mathbf{p}) = \begin{cases} \nabla\rho(\mathbf{p}_r, \mathbf{p}_o), & \text{if } |\mathbf{F}_{\text{att}}(\mathbf{p}_r)| > |\mathbf{F}_{\text{rep}}(\mathbf{p}_r)|, \\ & \quad \& \ |\mathbf{p}_r - \mathbf{p}_0| \\ & \quad\quad \le s_r \cdot T_s + r_r + r_o \\ & \quad \& \ \nabla\rho(\mathbf{p}_r, \mathbf{p}_o) \\ & \quad\quad = \nabla\rho(\mathbf{p}_r, \mathbf{p}_g) \\ \mathbf{0}, & \text{if } \mathbf{F}_{\text{att}}(\mathbf{p}_r) = \mathbf{F}_{\text{att}}(\mathbf{p}_r) = \mathbf{0} \\ \dfrac{\mathbf{F}_{\text{att}}(\mathbf{p}) + \mathbf{F}_{\text{rep}}(\mathbf{p})}{|\mathbf{F}_{\text{att}}(\mathbf{p}) + \mathbf{F}_{\text{rep}}(\mathbf{p})|}, & \text{elsewhere}. \end{cases} \tag{24}$$

Note that the new potential functions are only for robot collision, and the local minima problem still remains. In the next subsection, we propose the algorithm for local minima escape.

3.2 Random Force Algorithm for Local Minima Escape

3.2.1 Recognition of Local Minima Trap

On the conditions of constant speed and SAROG, the local minima problem is categorized into two

cases. Figure 9 illustrates the two cases of local minima trap. One case is that a robot is trapped in local minima before arriving a goal (i.e. oscillating across non-goal area). The other case is that a robot is trapped after arriving a goal (i.e. oscillating across a goal). Thus, in order to deal with the local minima trap, a robot should first recognize whether it is trapped across a goal or non-goal area. As illustrated in Fig. 9a when a robot is trapped across a non-goal area, the attractive forces of positions A and B are formed with same direction, but the total forces of the two positions are formed with opposite direction. On the other hand, as illustrated in Fig. 9b when a robot is trapped across a goal, both the attractive forces and the total forces of positions A and B are formed with opposite direction. Thus, a robot is trapped across a non-goal when the conditions are formed as

$$\mathbf{F}^c_{\text{tot}}(\mathbf{A}) = -\mathbf{F}^c_{\text{tot}}(\mathbf{B}) \text{ and } \mathbf{F}^c_{\text{att}}(\mathbf{A}) = \mathbf{F}^c_{\text{att}}(\mathbf{B}), \quad (25)$$

and a robot is trapped across a goal when conditions are formed as

$$\mathbf{F}^c_{\text{tot}}(\mathbf{A}) = -\mathbf{F}^c_{\text{tot}}(\mathbf{B}) \text{ and } \mathbf{F}^c_{\text{att}}(\mathbf{A}) = -\mathbf{F}^c_{\text{att}}(\mathbf{B}). \quad (26)$$

On the local minima condition of Eq. 26, a robot should find the path to reach the exact goal. For a solution, [8] proposed new potential functions for the problem named goals nonreachable with obstacles nearby (GNRON). In this paper, once a robot moves near a goal, we manually declare that a robot reaches a goal, and focus on the local minima across non-goal.

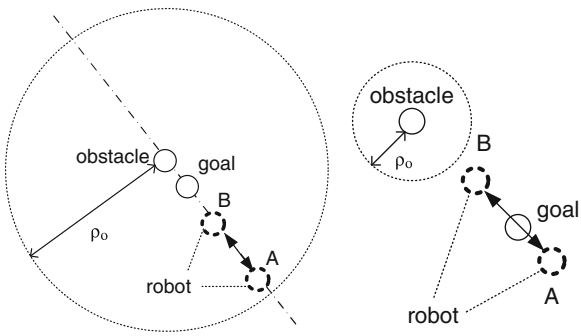

(a) A robot is trapped before arriving a goal.

(b) A robot is trapped after arriving a goal.

Fig. 9 Illustration: two cases of local minima trap on SAROG and constant robot speed

3.2.2 Random Force Algorithm for Local Minima Across Non-Goal

On the condition of Eq. 25, a robot should find the path to escape the local minima. For the path, we use a random unit total force (RUTF). The RUTF determines the robot direction and the robot escapes the local minima. After the RUTF based robot movement, the original potential force is continuously used until the condition of Eq. 25 arises. Thus, the random force algorithm alternates potential based motions with the random motion.

However, the RUTF may cause a robot to be collided with an obstacle if the random force is generated within the direction between $+\theta_u$ and $-\theta_u$ as illustrated in Fig. 10a. Thus, the RUTF

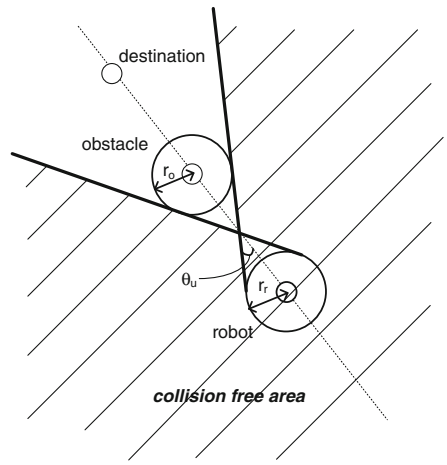

(a) The RUTF is generated within the direction between $+\theta_u$ and $-\theta_u$.

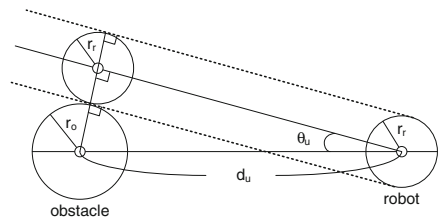

(b) The RUTF angle θ_u is formulated as (29) with d_u, r_r and r_o

Fig. 10 Illustration of RUTF angle formulation

should be generated in the collision free area as

$$\theta_u < \theta(\mathbf{F}^c_{\text{att}}) < \pi \quad \text{or} \quad -\pi < \theta(\mathbf{F}^c_{\text{att}}) < -\theta_u. \tag{27}$$

Given the obstacle and robot sizes, the angle θ_u is formulated with d_u, r_r and r_o as

$$\frac{r_r + r_o}{\sin\theta_u} = d_u, \tag{28}$$

$$\theta_u = \csc\left(\frac{r_r + r_o}{d_u}\right). \tag{29}$$

Thus, the RUTF for collision avoidance should be generated as

$$\csc\left(\frac{r_r + r_o}{d_u}\right) < \theta(\mathbf{F}^c_{\text{att}}) < \pi \quad \text{or}$$
$$-\pi < \theta(\mathbf{F}^c_{\text{att}}) < -\csc\left(\frac{r_r + r_o}{d_u}\right). \tag{30}$$

Figure 11 shows the effect of the RUTF based algorithm. A robot starts to move from (1.0 m, 1.0 m) with an obstacle positioned at (3.0 m, 3.0 m) and a goal positioned at (4.0 m, 4.0 m). The robot moves toward the goal of point (4.0 m, 4.0 m) with $s_r = 0.4$ m/s and $T_s = 1$ s. When the forces to exerting the robot are satisfied with Eq. 25, a robot recognizes the local minima across non-goal. Then, we exert a random unit total force (RUTF) onto a robot as shown in Fig. 11a. The RUTF helps a robot escape from the oscillation. After escaping from the oscillation, the robot continuously moves toward the goal of point (4.0 m, 4.0 m) by potential based forces as shown in Fig. 11b.

However, the RUTF based local minima escape is not applicable when a robot is positioned closer to a goal than an obstacle: the placement order is robot-goal-obstacle. To illustrate the case, consider that a robot is positioned at (1.0 m, 1.0 m), an obstacle is positioned at (3.4 m, 3.4 m) and a goal is positioned at (3.0 m, 3.0 m) as shown in Fig. 12a. From the time-instants 0–6, a robot moves close to a goal. At time-instant 6, the local minima across non-goal is satisfied with Eq. 25, and the RUTF with Eq. 30 exerts onto a robot resulting in the movement as shown in Fig. 12b. After the robot escapes from the local minima, the robot continuously moves by potential based forces as shown in Fig. 12b–d, where the robot moves back to the local minima. That is, the RUTF based local minima escape is applicable

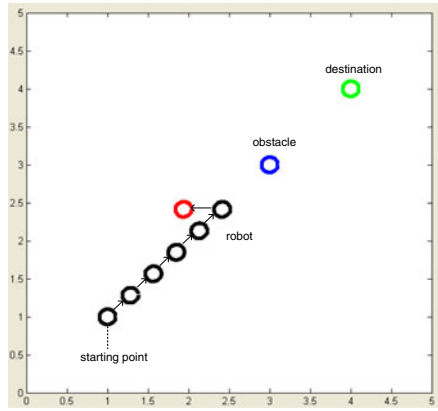

(a) The robot moves from (1.0m, 1.0m) to (4.0m, 4.0m) with $s_r = 0.4m/s$ and $T_s = 1s$.When the forces to exerting the robot are satisfied with (25), we exert RUTF onto a robot.

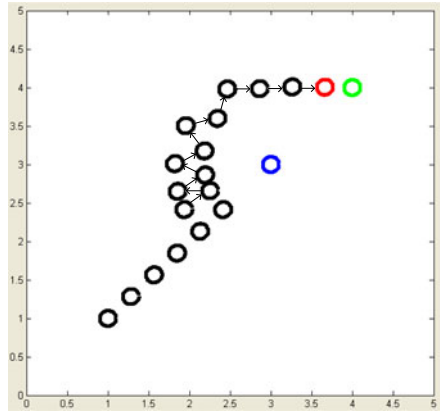

(b)The RUTF helps arobot escape the local minima, and the robot continuously moves toward the goal (4.0m, 4.0m) by potential based forces.

Fig. 11 Local minima escape using RUTF

only when $\rho(\mathbf{p}_r, \mathbf{p}_g) > \rho(\mathbf{p}_r, \mathbf{p}_o)$. Otherwise, a robot moves back to previous local minima as shown in Fig. 12d.

Thus, in the case of $\rho(\mathbf{p}_r, \mathbf{p}_g) < \rho(\mathbf{p}_r, \mathbf{p}_o)$, we use a potential function with repulsion removal as

$$\mathbf{F}^c_{\text{tot}}(\mathbf{p}) = \begin{cases} \mathbf{0}, & \text{if } \mathbf{F}^c_{\text{att}}(\mathbf{p}) = \mathbf{0} \\ \dfrac{\mathbf{F}^c_{\text{att}}(\mathbf{p})}{|\mathbf{F}^c_{\text{att}}(\mathbf{p})|}, & \text{otherwise,} \end{cases} \tag{31}$$

That is, once the potential forces and the distance conditions are both satisfied with Eq. 25 and $\rho(\mathbf{p}_r, \mathbf{p}_g) < \rho(\mathbf{p}_r, \mathbf{p}_o)$, the RUTF changes robot direction and the potential force of Eq. 31 exerts

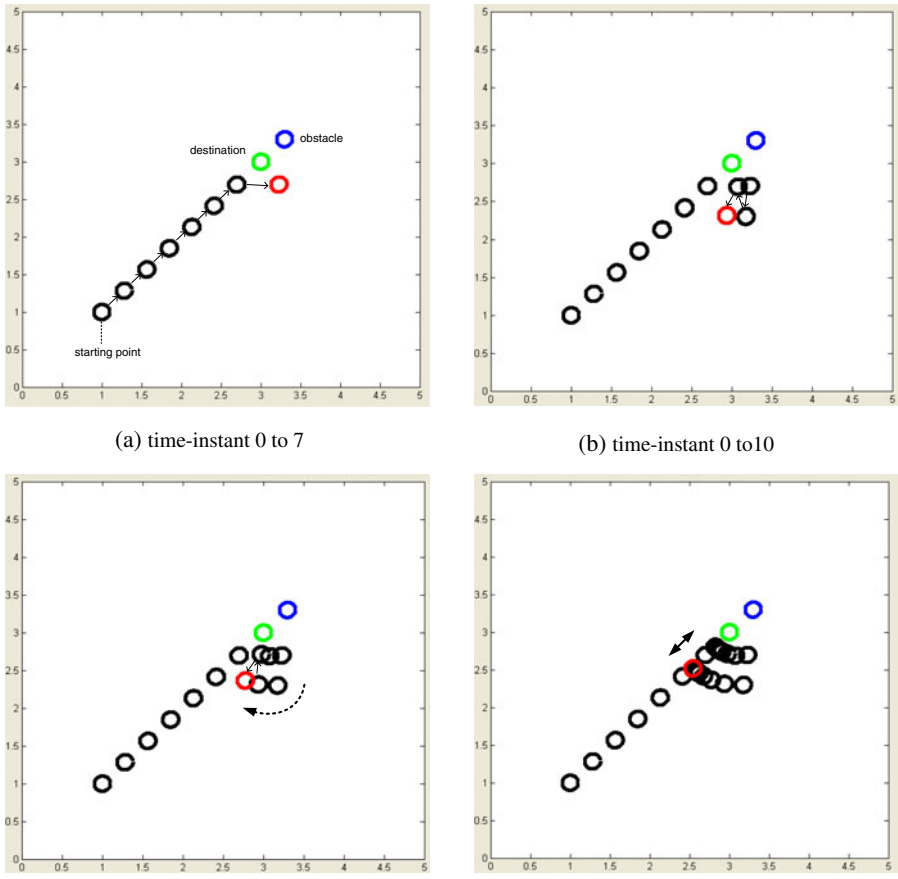

(a) time-instant 0 to 7

(b) time-instant 0 to10

(c) time-instant 0 to 12

(d) time-instant 0 to 20

Fig. 12 RUTF algorithm limitation: Even though the RUTF exerts onto a robot, the robot eventually moves back to the local minima of SAROG

onto a robot. The RUTF and the potential function with removal (RUTF-RR) algorithm derives a robot to reach a goal by removing a repulsion force since the movement back to previous local minima after RUTF is from the repulsive force existence. The attractive force exertion of Eq. 31 continues until a robot arrives at a goal.

When the RUTF-RR is used, the robot collision issue should be considered as well. Since the robot moves with only attractive force, it is possible for the robot to collide with an obstacle. The collision occurs more frequently when the size of a robot and/or an obstacle increases, and the distance between a goal and an obstacle becomes shorter. In order to investigate the anti-collision condition, Fig. 13a illustrates the placement and the size of a robot, a goal and an obstacle. Given the robot position $\mathbf{P}_r$, the RUTF should be generated in the collision free area. Then, after the RUTF exertion to the collision free area, the collision is prevented even with the attraction force only. Figure 13a is re-illustrated in Fig. 13b to find the anti-collision condition. The angles θ_1 and θ_2 are formulated with r_r, r_o and d_v as

$$\frac{r_r + r_o}{\sin\theta_1} = \frac{r_r + r_o}{\sin\theta_2} = d_v, \tag{32}$$

$$\theta_1 = \theta_2 = \csc\left(\frac{r_r + r_o}{d_v}\right). \tag{33}$$

Then, the shortest distance d_w between a robot and the shaded region boundary is

$$\frac{d_w}{\sin\theta_1} = d_u, \tag{34}$$

$$d_w = d_u \cdot \sin\theta_1. \tag{35}$$

In addition, the RUTF angle $\theta\left(\mathbf{F}^c_{\text{tot}}\right)$ is

$$\theta\left(\mathbf{F}^c_{\text{tot}}\right) = \pi - \theta_1. \tag{36}$$

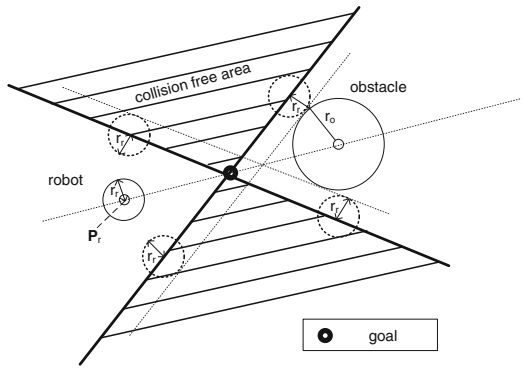

(a) Illustration of the placement and the size of a robot, a goal and an obstacle

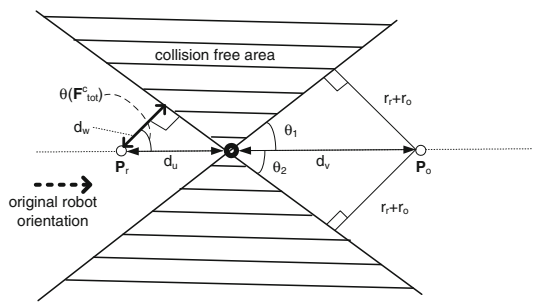

(b) Geometry for d_w and $\theta(\mathbf{F}^c_{tot})$

Fig. 13 Illustration of the anti-collision condition

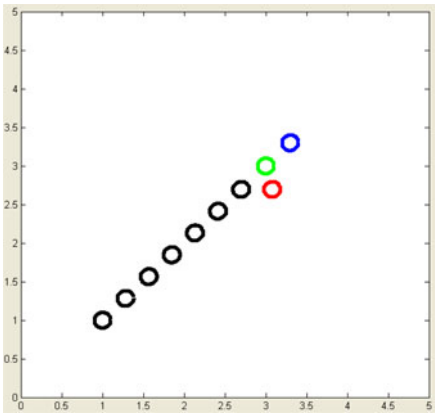

(a) At time-instant 7

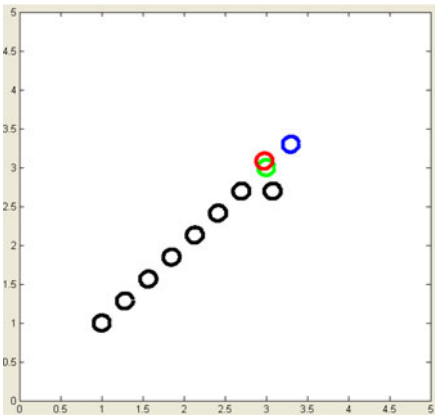

(b) At time-instant 8

Fig. 14 Random unit total force with repulsion removal (RUTF-RR)

In order to move inside the shaded region with speed s_r, the robot should keep moving with the force direction $\pm(\pi - \theta_1)$ for τ time-instants, where

$$\tau = \left\lceil \frac{d_w}{s_r} \right\rceil. \tag{37}$$

The sign $\pm$ of the force direction is randomly assigned. After τ time-instants, a robot keeps moving by the attraction only.

Figure 14 shows the one realization based on same simulation condition of Fig. 12. In Fig. 14a, the forces exerting onto a robot and the distance condition are both satisfied with Eq. 25 and $\rho(\mathbf{p}_r, \mathbf{p}_g) < \rho(\mathbf{p}_r, \mathbf{p}_o)$ at time-instant 6. At time-instant 7, the RUTF is exerting onto a robot to the collision free area. In Fig. 14b, at time-instant 8, the attractive force only in Eq. 31 is exerting onto a robot, and the robot finally reaches the goal without the movement back to the local minima.

3.3 Algorithm Summary and Finite State Representation

To summarize, we represent the whole algorithms with a finite state data flow as illustrated in Fig. 15. It shows that a robot moves based on six different states: potential function based navigation with Eq. 24, GNRON navigation [8], RUTF based navigation with Eq. 30, RUTF-RR preparation navigation with Eq. 36, RUTF-RR navigation with Eq. 31 and goal (stop).

As an initial stage, a robot continuously moves with potential function based navigation of Eq. 24 until $\mathbf{F}^c_{\text{tot}}(n) = -\mathbf{F}^c_{\text{tot}}(n-1)$. At time n, if the condition of $\mathbf{F}^c_{\text{att}}(n) = -\mathbf{F}^c_{\text{att}}(n-1)$ is satisfied, a robot recognizes its situation as either local minima or GNRON. Simultaneously, if the con-

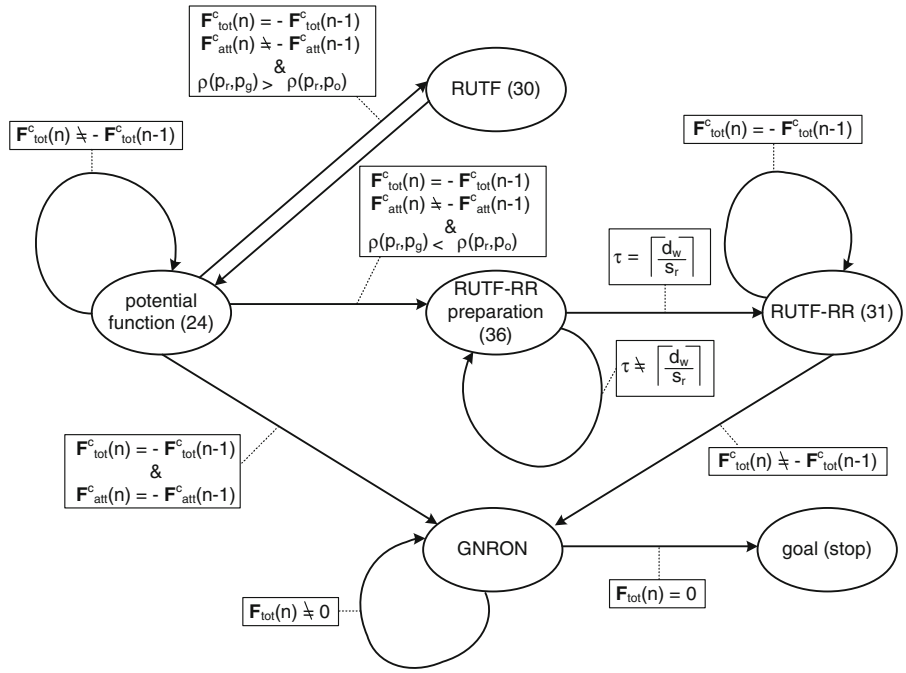

Fig. 15 Finite state representation which classifies the robot movement into six states

dition of $\rho(\mathbf{p}_r, \mathbf{p}_g) > \rho(\mathbf{p}_r, \mathbf{p}_o)$ is satisfied, a robot is trapped in local minima, and the RUTF based navigation of Eq. 30 determines the robot direction. Once a robot escapes the local minima, the navigation state goes back to potential function based navigation. On the other hand, if the conditions of $\mathbf{F}^c_{\text{att}}(n) = -\mathbf{F}^c_{\text{att}}(n-1)$ and $\rho(\mathbf{p}_r, \mathbf{p}_g) < \rho(\mathbf{p}_r, \mathbf{p}_o)$ are simultaneously satisfied, the RUTF-RR preparation navigation of Eq. 36 exerts on a robot during the time-instants $\left\lceil \frac{d_w}{s_r} \right\rceil$. After the time-instants $\left\lceil \frac{d_w}{s_r} \right\rceil$, the RUTF-RR navigation of Eq. 31 exerts on a robot until $\mathbf{F}^c_{\text{tot}}(n) = -\mathbf{F}^c_{\text{tot}}(n-1)$. The condition of $\mathbf{F}^c_{\text{tot}}(n) = -\mathbf{F}^c_{\text{tot}}(n-1)$ represents GNRON, where a robot reaches a goal nearby and moves across a goal. The GNRON navigation is also enabled with the condition $\mathbf{F}^c_{\text{tot}}(n) = -\mathbf{F}^c_{\text{tot}}(n-1)$ from the state of potential function based navigation. At last, a robot stops when $\mathbf{F}_{\text{tot}}(n) = 0$.

4 Algorithm Verification and Analysis

4.1 Simulation Setup

For the algorithm verification, we used the WiRobot X80 as shown in Fig. 16. The X80 underlies technology evolved from Dr Robot Distributed Computation Robotic Architecture, originally developed for Dr Robot Humanoid Robot. It is developed for fast and strong mo-

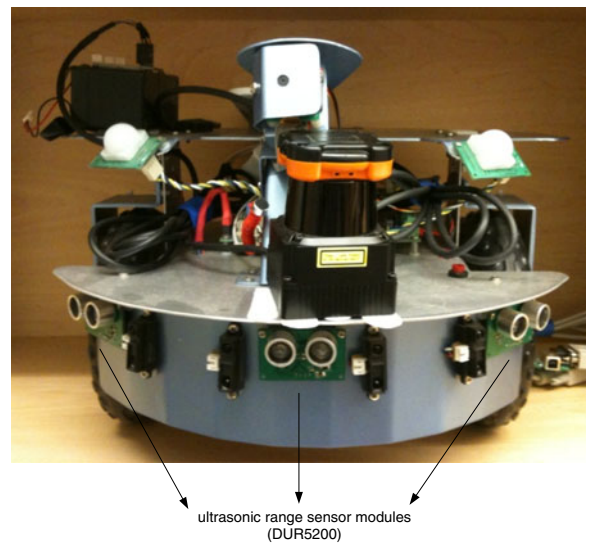

Fig. 16 WiRobot X80 evolved from Dr Robot Distributed Computation Robotic Architecture, originally developed for Dr Robot Humanoid Robot: For the estimating the distance between a robot and an obstacle, three ultrasonic range sensor modules of DUR5200 are attached to the robot

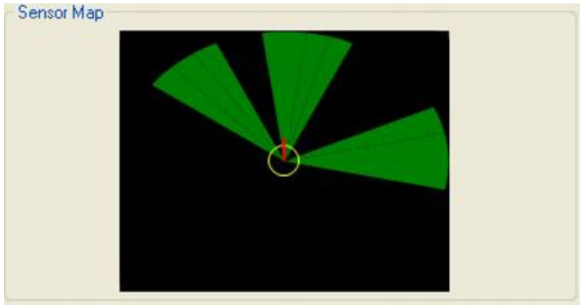

Fig. 17 The range sensor modules DUR5200 searches its surrounded environment

tion, while itself remaining lightweight and nimble. The wheel-based platform is with two 12V DC motors each supply 22 kg·cm of torque to the 18-cm wheels, yielding a top speed in excess of 1 m/s. Two high-resolution with 1,200 counts per wheel cycle quadrature encoders mounted on each wheel provide high-precision measurement and control of wheel movement.

For estimating the distance between a robot and an obstacle, we equipped the robot with three ultrasonic range sensor modules of DUR5200. The range sensor detects an obstacle within 3.4 m as shown in Fig. 17. The distance data is precisely presented by the time interval between the time-instant when the measurement is enabled and the time-instant when the echo signal is received. By using the ultrasonic range sensor modules, the robot recognizes its near obstacle position up to 3.4 m. For the proposed algorithm verification on the restricted two conditions of SAROG and robot constant speed, we set up the robot, obstacles and the goal as in Figs. 18 and 19.

In the first test, we verify our proposed algorithm of the finite state navigation with multiple states by showing three different goals. For each goal, the robot selects different navigation states. For *goal 1*, four states of potential function, RUTF, GNRON and goal were switched. For *goal 2*, three states of potential function, GNRON and goal were switched. For *goal 3*, six states of potential function, RUTF, RUTF-RR preparation, RITF-RR, GNRON and goal were switched. Through the three goals, we show that the robot automatically switched the different navigation states according to the positions of a robot, an obstacle and a goal. Initially, *goal 1* is enabled while *goal 2* and *goal 3* are disabled.

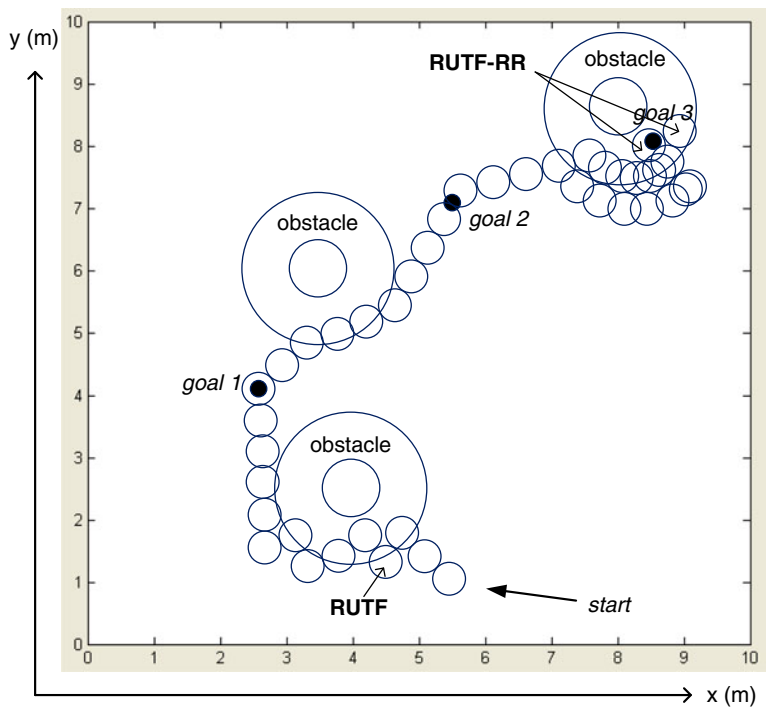

Fig. 18 WiRobot X80 traveled from *Start* to *goal 1*, *goal 2* and *goal 3* in order. During the navigation, RUTF and RUTF-RR algorithms are used for local minima escape

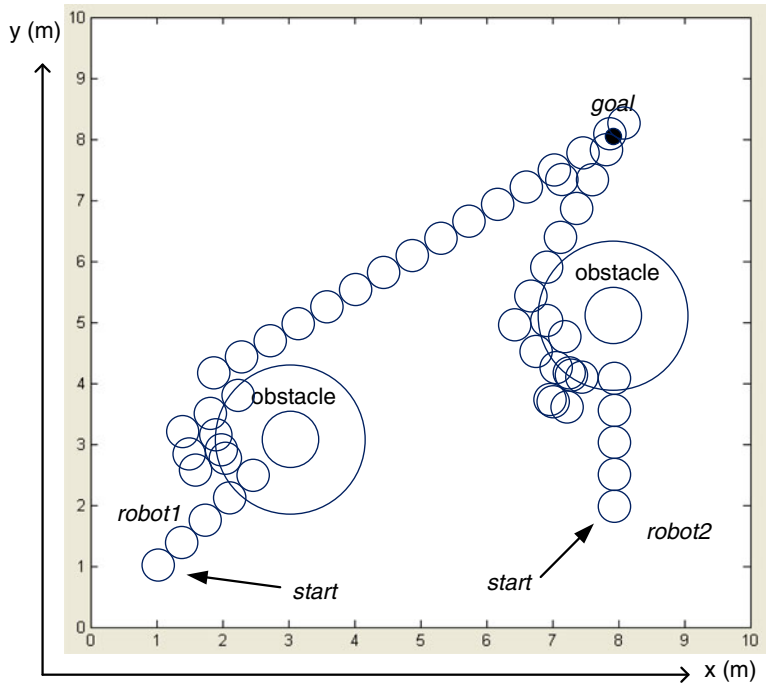

Fig. 19 Two WiRobot X80s traveled to the same goal. During the navigation, each robot is aided by RUTF, but the average navigation speeds are different due to RUTF direction

After the robot reaches *goal 1*, *goal 2* only is enabled. Finally, after the robot reaches *goal 2*, *goal 3* only is enabled. For the navigation to *goal 1*, the robot has the problem on SAROG; and thus, will be trapped on local minima by using potential field method only. In the local minima trap, we will show the RUTF will solve the problem. For the navigation to *goal 3*, the robot also has the problem on SAROG; and thus will be trapped on local minima again. However, in the case, the RUTF cannot solve the problem; the robot moves back to original local minima after RUTF. In the local minima trap, we will show the RUTF-RR will solve the problem. The selection of RUTF, RUTF-RR and potential field method is determined by our proposed algorithm in Fig. 15 and Section 3.3.

In the second test, two robots simultaneously start for the navigation to *goal*. During the navigation, the two robots have the problem on SAROG; and thus, will be trapped on local minima by using potential field method only. In each local minima trap, we will show the RUTF will solve the problem. Especially, in this test, we will evaluate the navigation time and investigate the effect of RUTF direction.

4.2 Results and Discussion

As depicted in Fig. 18, in the first test, X80 traveled from *Start* to three goals; *goal 1* positioned at (2.5 m, 4.0 m), *goal 2* positioned at (5.5 m, 7.0 m) and *goal 3* positioned at (8.5 m, 8.0 m). Each obstacle is positioned at (4.0 m, 2.5 m), (3.5 m, 6.0 m) and (8.0 m, 8.5 m) with $r_o = 0.4375$ m and $\rho_o = 1.2$ m. The robot starts from the position (5.5 m, 1.0 m) with $r_r = 0.25$ m, $T_s = 1$ s and $s_r = 0.5$ m/s. With *goal 1* only enabled, the robot first moved toward *goal 1* with potential functions and kept moving until the condition of Eq. 25 is satisfied at time 2 (s). At time 2 (s), the robot compared the distance condition, which was $\rho(\mathbf{p}_r, \mathbf{p}_g) > \rho(\mathbf{p}_r, \mathbf{p}_o)$, and RUTF instead of the potential functions determined robot direction for the local minima escape. From 3 (s) to 13 (s), the robot moved toward *goal 1* by using the potential field, and finally arrived at *goal 1*. Once the robot arrived at *goal 1*, *goal 1* was disabled and only *goal 2* was enabled. We set the starting time from *goal 1* to zero. From *goal 1* to *goal 2*, any local minima problem did not occur. Note until time 2 (s), the robot has the potential function involved with attraction force only. From time

2 (s) to 6 (s), the potential function involved both the attraction force and the repulsion force since the robot positioned within the obstacle influence. From 6 (s) to 9 (s), the potential function involved with attraction force only and the robot finally arrived at *goal 2*. Similarly, once the robot arrived at *goal 2*, *goal 2* was disabled and only *goal 3* was enabled. We also set the starting time from *goal 2* to zero. From *goal 2* the robot moved toward *goal 3* with potential functions and kept moving until the condition of Eq. 25 is satisfied at time 15 (s). At time 15 (s), the robot compared the distance condition, which was $\rho(\mathbf{p}_r, \mathbf{p}_g) < \rho(\mathbf{p}_r, \mathbf{p}_o)$, and RUTF-RR instead of the potential functions determined robot direction for the local minima escape, and finally let the robot arrived at *goal 3* with $\tau = 1$.

Through the random force based algorithms of RUTF and RUTF-RR, we showed that the robot escaped the local minima trap and avoided robot-obstacle collision on the SAROG and robot constant speed. In addition, each algorithm such as RUTF, RUTF-RR and potential functions was adaptively selected based on the conditions of Eq. 25, $\rho(\mathbf{p}_r, \mathbf{p}_g) < \rho(\mathbf{p}_r, \mathbf{p}_o)$ and $\rho(\mathbf{p}_r, \mathbf{p}_g) > \rho(\mathbf{p}_r, \mathbf{p}_o)$, and its whole algorithm was summarized in Fig. 15 and Section 3.3.

As depicted in Fig. 19, in the second test, two X80s traveled from different positions at (1.0 m, 1.0 m) and (8.0 m, 2.0 m) to the *goal* positioned at (8.0 m, 8.0 m). All other conditions such as r_r, T_s and s_r are same as ones in the first test. The *robot 1* first moved toward *goal* with potential functions and kept moving until the condition (25) is satisfied at time 4 (s). At time 4 (s), the robot compared the distance condition, which was $\rho(\mathbf{p}_r, \mathbf{p}_g) > \rho(\mathbf{p}_r, \mathbf{p}_o)$, and RUTF instead of the potential functions determined robot direction for the local minima escape. From 5 (s) to 27 (s), the robot moved toward the *goal* by using the potential field, and finally arrived at *goal*. Similarly, the *robot 2* first moved toward *goal* using potential functions, and RUTF determined robot direction for the local minima escape at 4 (s). From 5 (s) to 22 (s), the robot moved toward the *goal* by using the potential field, and finally arrived at *goal*. Note that the *robot 1* moves 9.9 m for 27 (s) while *robot 2* moves 6.0 m for 22 (s) (i.e. 0.367 m/s with *robot 1* and 0.273 m/s with *robot 2*). The average navigation speed is affected by RUTF direction, $\theta(\mathbf{F}^c_{\text{att}})$. Thus, the optimal $\theta(\mathbf{F}^c_{\text{att}})$ should be considered for the fast navigation. Furthermore, SAROG problem in the dynamic conditions such as moving obstacles are worthy for consideration as in the future work.

5 Conclusion

We have described new problem of symmetrically aligned robot-obstacle-goal (SAROG) with constant robot speed when using potential field methods for mobile robot path planning. For dealing with the corresponding two potential risks of robot-obstacle collision and local minima trap, new potential functions and random force based algorithms have been proposed. In addition, for a complete navigation on SAROG and constant speed, we have shown the finite state representation with six navigation states. Finally, the algorithm has been verified using WiRobot X80 with three ultrasonic range sensor modules.

Acknowledgements This research is supported by the Ubiquitous Computing and Network (UCN) project, Knowledge and Economy Frontier R&D Program of the Ministry of Knowledge Economy (MKE) in Korea as a result of UCN's subproject 11C3-T3-50S.

References

1. Dudek, G., Jenkin, M.: Computational Principles of Mobile Robotics. Cambridge University Press, Cambridge (2000)
2. Veelaert, P., Bogaerts, W.: Ultrasonic Potential Field Sensor for Obstacle Avoidance. IEEE Trans. Robot. Autom. **15**, 774–779 (1999)
3. Damas, B., Lima, P., Custodio, L.: a modified potential fields method for robot navigation applied to dribbling in robotic soccer. In: Proceddings of RoboCup 2002 Symposium. Fukuoka, Japan (2002)
4. Latombe, J.: Robot Motion Planning. Kluwer, Norwell (1991)
5. Tilove, R.: Local obstacle avoidance for mobile robots based on the method of artificial potentials. In: Proceedings of the IEEE Conference on Robotics and Automation, pp. 566–571. Cincinnati, Ohio (1990)
6. Chengqing, L., Ang, M.H., Krishnan, H., Yong, L.S.: Virtual obstacle concept for local-minimum-recovery in potential-field based navigation. In: Proceedings of the IEEE Conference on Robotics and Automation, pp. 983–988. San Francisco, CA (2000)

7. Koren, Y., Borenstein, J.: Potential field methods and their inherent limitations for mobile robot navigation. In: Proceedings of the IEEE Confernce on Robotics and Automation, pp. 1398–1404. Sacramento, California (1991)
8. Ge, S., Cui, Y.: Dynamic motion planning for mobile robots using potential field method. Auton. Robots **13**, 207–222 (2002)
9. Ge, S., Cui, Y.: New potential functions for mobile robot path planning. IEEE Trans. Robot. Autom. **16**(5), 615–620
10. Connolly, C., Burns, J., Weiss, R.: Path planning using Lapace's equation. In: Proceedings of the IEEE International Conference on Robotics and Automation, pp. 2102–2106 (1990)
11. Rimon, E., Koditscheck, D.: Exact robot navigation using artificial potential functions. IEEE Trans. Robot. Autom. **8**(5), 501–518 (1992)
12. Singh, L., Wen, J., Stephanou, H.: Real-time robot motion control with circulatory fields. In: Proceedings of the IEEE International Conference on Robotics and Automation, pp. 2737–2742 (1996)
13. Ren, J., McIsaac, K.A., Patel, R.V.: Modified Newton's method applied to potential field-based navigation for mobile robots. IEEE Trans. Robot. **22**(2), 384–390 (2006)
14. Chang, H.: A new technique to handle local minimum for imperfect potential field based motion planning. In: Proceedings of the IEEE International Conference on Robotics and Automation, pp. 108–112 (1996)
15. Caselli, S., Reggiani, M., Rocchi, R.: Heuristic methods for randomized path planning in potential fields. In: Proceedings of the IEEE International Symposium on Computational Intelligence in Robotics and Automation, pp. 426–431 (2001)
16. Barraquand, J., Latombe, J.C.: Robot motion planning: a distributed representation approach. Int. J. Rob. Res. **10**(6), 628–649 (1991)
17. Barraquand, J., Langlois, B., Latombe, J.C.: Numerical potential field techniques for robot path planning. IEEE Trans. Syst. Man Cybern. **22**(2), 224–241 (1992)
18. Ordonez, C., Collins, E.G., Selekwa, M.F., Dunlap, D.D.: The virtual wall approach to limit cycle avoidance for unmanned ground vehicles. In: Robot. Auton. Syst. (Elsevier) **56**, 645–657 (2008)
19. Olunloyo, V.O.S., Ayomoh, M.K.O. Autonomous mobile robot navigation using hybrid virtual force field concept. Eur. J. Sci. Res. **31**(2), 204–228 (2009)
20. http://www.pages.drexel.edu/~weg22/ER1.html
21. Borenstein, J., Koren, Y.: Real-time obstacle avoidance for fast mobile robots. IEEE Trans. Syst. Man Cybern. **19**, 1179–1187 (1989)
22. Chuang, J.H., Ahuja, N.: An analytically tractable potential field model of free space and its application in obstacle avoidance. IEEE Trans. Syst. Man Cybern. B **28**, 729–736 (1998)